

# Spicule movement on RBCs during echinocyte formation and possible segregation in the RBC membrane

K.A. Melzak<sup>a,\*</sup>, S. Moreno-Flores<sup>b</sup>, K. Bieback<sup>c,\*</sup>

<sup>a</sup> Institute of Functional Interfaces, Karlsruhe Institute of Technology, Eggenstein-Leopoldshafen, Germany

<sup>b</sup> Vienna, Austria

<sup>c</sup> Institute for Transfusion Medicine and Immunology, Flowcore Mannheim, Medical Faculty Mannheim, Heidelberg University, Mannheim, Germany

## ARTICLE INFO

### Keywords:

Bilayer deformations  
Shape transformations  
Domains  
Erythrocytes  
Line tension  
Membrane

## ABSTRACT

We use phase contrast microscopy of red blood cells to observe the transition between the initial discocyte shape and a spiculated echinocyte form. During the early stages of this change, spicules can move across the surface of the cell; individual spicules can also split apart into pairs. One possible explanation of this behaviour is that the membrane forms large scale domains in association with the spicules. The spicules are formed initially at the rim of the cell and then move at speeds of up to 3  $\mu\text{m}/\text{min}$  towards the centre of the disc. Spicule formation that was reversed and then allowed to proceed a second time resulted in spicules at reproducible places, a shape memory effect that implies that the cytoskeleton contributes towards stopping the spicule movement. The splitting of the spicules produces a well-defined shape change with an increase in membrane curvature associated with formation of the daughter pair of spicules; the total boundary length around the spicules also increases. Following the model in which the spicules are associated with lipid domains, these observations suggest an experimental procedure that could potentially be applied to the calculation of the line tension of lipid domains in living cells.

## 1. Introduction

Red blood cells (RBCs) exhibit a range of different cell shapes that are associated with changes in the relative areas of the inner and outer leaflets of the cell membrane [1,2]. The familiar biconcave disc shape of healthy red blood cells is lost as the outer leaflet of the membrane expands relative to the inner leaflet: the excess area is accommodated by the formation of convex bumps on the surface of the cell. The resulting spiculated form is called an echinocyte.

As RBCs age during storage, the bumps appear first as ripples around the rim of disc shaped cells [3]; spicules then appear on the top and bottom surfaces of the disc; the cells become rounder, and the spicules become more numerous and finer (Fig. 1). The discocyte to echinocyte transition can be driven by multiple factors, including the decrease of ATP levels during storage [4], as well as increased pH levels associated with proximity to soda lime glass, and multiple other factors [5].

Models that reproduce the shapes of discocytes can be created by considering the energetic contributions of the bilayer alone [6]: the

shape with the energetic minimum matches well with the observed shape of the discocyte [6,7]. The spiculated echinocyte forms can be described accurately using models in which the relative area difference of the inner and outer leaflets of the bilayer is varied, but only if the contributions of the cytoskeleton are also considered [2,3,7,8]. For area differences that are relatively low (i.e., for positive curvatures that are fairly low), it is possible to find minima in the membrane energy without considering the cytoskeleton, but these do not correspond to the familiar echinocyte shapes [8].

Echinocyte and discocyte shapes can both be modeled using uniform values for the membrane mechanical properties: single values are used for parameters such as the bending modulus or the resistance to shear stretching. The models thus produced can describe the different cell shapes and can also explain the formation of vesicles, an event which is predicted if the positive curvature is sufficiently high and if the cytoskeleton is not considered, or if it has detached from the bilayer. In this case, there is no energy minimum to provide a stable shape, and an increasing area difference between the inner and outer leaflets causes the membrane to proceed in the direction of budding [9].

\* Corresponding authors.

E-mail addresses: kathryn.melzak@kit.edu (K.A. Melzak), Karen.Bieback@medma.uni-heidelberg.de (K. Bieback).

<sup>1</sup> Postal address: Institut für Funktionelle Grenzflächen (IFG), Gebäude 330, Karlsruher Institut für Technologie (KIT), Hermann-von-Helmholtz-Platz 1, 76344 Eggenstein-Leopoldshafen, Germany.

<sup>2</sup> Postal address: Friedrich-Ebert-Str. 107, Institute of Transfusion Medicine and Immunology, Medical Faculty, Mannheim, Germany

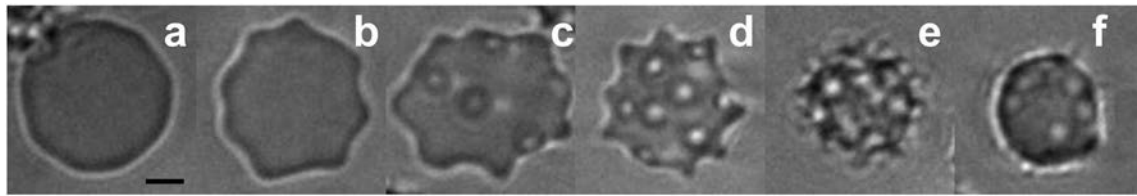


**Fig. 1.** Typical sequence of shapes observed as RBCs are stored for increasing lengths of time (scale bar 2.5  $\mu\text{m}$ ). The initial biconcave disc of the RBC discocyte (a) develops bumps around the rim (b), then over the top and bottom surfaces (c); the overall disc shape is lost as the cells become round (d); spicules become more prominent and then become finer (e, f).

Events such as fusion or fission of features within the plane of the cell surface are, however, not as readily explained by membranes with uniform properties. Such events are seen in giant vesicle model systems composed of ternary lipid mixtures, where large scale lipid domains have been observed to form, coalesce, and localise according to curvature [10,11]. The large scale domains seen in these cases have chemically distinct compositions, with domain specific mechanical properties that can affect the overall vesicle shape [12].

One of the features that controls the behaviour of lipid domains in model systems is the line tension, which results from differences in the bilayer thickness at the domain boundaries, and the molecular distortions that occur to correct this mismatch [13]. If the line tension is sufficiently high, it leads to the formation of circular domains that minimise the boundary length and thus minimise the line energy. Domains that are sufficiently large and that have a low enough resistance to out of plane bending (i.e. low bending modulus) can reduce the line length to zero by budding to form a vesicle composed of one of the lipid domains. The shapes of the domains will therefore be a result of a balance of the line tension and the bending modulus [12].

In the work presented here, we observe the shape changes associated with the early stages of the transition between the initial biconcave discocyte form of RBCs and the spiculated echinocyte forms. We use phase contrast microscopy of unlabeled cells, which enables us to observe dynamic events on cells with minimal interference of external agents that could affect the cell behaviour. The goals here are to characterise the nature of the spicules and the spicule behaviour, and also to use the spicule splitting events to demonstrate an approach to investigate membrane energetics.

## 2. Materials and methods

### 2.1. Red blood cells

Blood was collected from donors that had provided informed consent and the experiments were approved by the Medical Ethics Committee of the university. The RBCs were washed  $3 \times$  in phosphate buffered saline (PBS) prepared from tablets (VWR; PBS solution was 137 mmol/l sodium chloride, 2.7 mmol/l potassium chloride, and 10 mmol/l phosphate pH 7.4). All RBCs were refrigerated before use, in accordance with the standard Red Cross procedures for transportation and storage of blood samples. Samples were stored for a maximum of four days before use. The storage times for the individual samples are given in the figure legends below the image sequences in the supporting information.

### 2.2. Adhesive substrate

Glass slides with a depression (Häberle, Lonsee Ettlenschieß, Germany) were modified with poly(allylamine hydrochloride) (PAH) as described previously [7,14]. Slides that had been cleaned with a solution of ammonium hydroxide and  $\text{H}_2\text{O}_2$  at  $70^\circ\text{C}$  were incubated for 30 min in a 0.1 g/ml solution of PAH (Aldrich, average Mw 15,000 Da) in 0.5 mol/l NaCl. The slides were then rinsed and stored in water. The adhesive layer serves to hold RBCs in place and also covers the glass of

the slide.

### 2.3. Microscopy

The RBCs were observed under phase contrast, using a Zeiss Axiovert A1 microscope ( $40\times$  objective, NA = 0.55) with a Zeiss AxioCam ICc1 camera, (Zeiss, Oberkochen, Germany). Images were acquired with a 100 ms exposure time. Images are shown here with no modification other than conversion from RGB to greyscale. A sample unmodified image is shown in the supporting information as Fig. S1. No anti vibration table was used.

### 2.4. Video files in the supporting material

The figures in the results typically show six frames from the sequences in which RBCs changed shape. The full sequences with all available images are included in the video files. The frame rate was kept constant and the videos therefore do not show the event times, which may be obtained from the figures. The final five frames from each sequence were held constant in the video sequences. Links to the video sequences may be found with the associated figures.

### 2.5. Formation of echinocytes

Up to 80  $\mu\text{l}$  of PBS was added to the depression in the PAH modified slide. A suspension of RBCs was added to the slide and the RBCs were allowed to settle to the surface. One field of view was selected and then monitored at room temperature over a period of less than 2 h. Images were acquired at intervals of about 1 min, or more frequently if an event was detected in progress. Formation of echinocytes was induced by incubation for sufficient periods of time in PBS or by addition of a coverslip, which increases the pH immediately adjacent to the coverslip, thus leading to the echinocyte formation through the “glass effect” [5]. One experiment was done with RBCs that had been incubated in a mixture of diethylhexylphthalate (DEHP) in PBS (Fig. 2d), and additional experiments were done in high salt conditions (Figs. 4, 5b).

Full details for each image sequence are given in the supporting information, including storage time in plasma and PBS suspension prior to the experiment. Figures in the supporting information show a  $50 \times 50 \mu\text{m}$  region around the cell of interest, as well as the initial appearance of the cells, or, if relevant, the appearance prior to addition of a coverslip.

### 2.6. Spicule circumferences and boundary lengths

The boundary length around the circumference of the spicules was determined using the Kappa plug in of ImageJ (<http://rsb.info.nih.gov/ij/>). Images of spicules before and after splitting events were acquired as described above; spicules were identified as circular regions that were brighter than the dark halo surrounding them. Splined curves produced from a set of manually selected control points on the images were then used to identify the spicule boundary. The boundary lengths were calculated as the average values of 3–5 such curves.

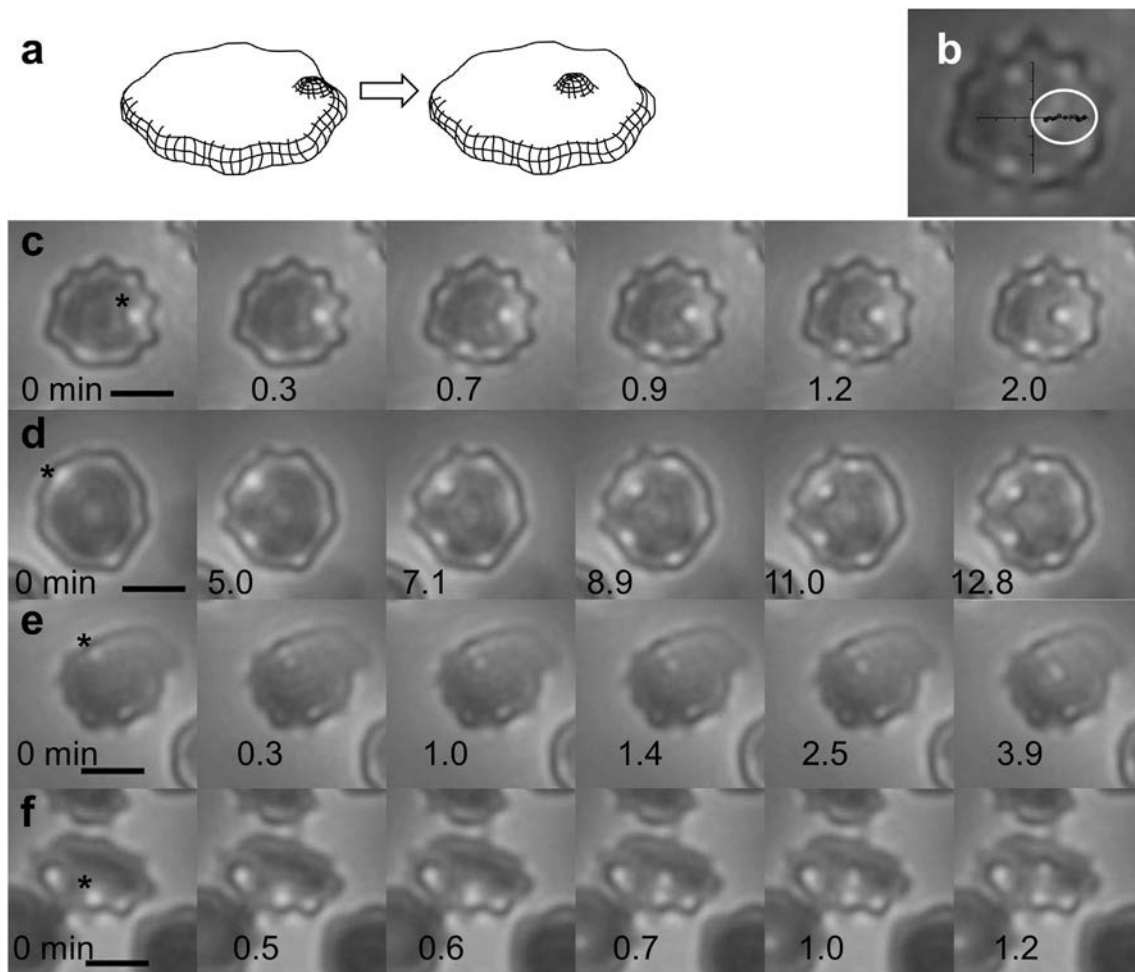


**Fig. 2.** Movement of spicules across the surface of RBCs. The typical pattern of movement is from the edge of the cell towards the centre, as indicated in the cartoon in 2a, and in the spicule track shown in the circled region in 2b. Selected images from the series of 2b are shown in row 2c. Row d shows a similar example; row e shows spicule movement in an RBC that had spontaneously deformed on the surface, as shown in the sequence in the supporting information; row f shows the spicule movement in a cell that is resting on another cell in the lower left corner of the images, giving it a slight tilt. The numbers show the time in minutes relative to the initial images, the scale bars show 5  $\mu\text{m}$ , and the asterisks on the initial images mark the positions of the moving spicules. Supporting information: video Fig. 2c 3c; video Fig. 2d; video Fig. 2e; video Fig. 2f.

### 3. Results

#### 3.1. Spicule movement

In order to demonstrate spicule movement, it is necessary to be able to distinguish between the movement across the surface of the RBCs and the movement of spicules that occurs as the RBCs change from the flattened shape of the early stage echinocytes (Fig. 1b and c) to the rounded form of the later stage echinocytes (Fig. 1d f). One experimental requirement is therefore to have RBCs that change shape relatively slowly, so that the overall cell profile shows little change during the period of observation.

The shape of RBCs is relatively stable on PAH surfaces. Previous experiments have shown that freshly collected and washed discocytes can maintain their smooth shape for at least 2 h [7]. For the experiments described here, the process of echinocyte formation was accelerated by a combination of storage of RBCs in plasma or buffer prior to use, and some degree of evaporation, which would increase the salt concentration in the medium; additionally, for some experiments, a glass coverslip was added, which increases the pH. All of these factors can contribute to driving echinocyte formation [5]. The effect of high salt concentration is described separately, below.

Typically, between 50 and 100 cells were visible within the field of

view. Under the experimental conditions used here, RBCs were largely discocytes or early stage echinocytes at the start of the experiments. Most of the cells adsorbed flat on the surface, presenting a circular profile; some cells adsorbed on edge; a small number adsorbed at a slight angle because they were resting on a second cell (see Fig. S1 in the supporting information showing a sample field of view). The cells were observed over some time, either with or without the addition of a coverslip. Without a coverslip, the observation of moving spicules was relatively infrequent, so that it was possible to follow two or three sets of deposited RBCs without capturing a moving spicule event. With the addition of a coverslip, examples of moving spicules were reliably generated within a single observation period.

The examples showing the greatest extent of spicule movement (sequences 2c and 2e) are shown in Fig. 2. Additional figures in the supporting information (Figs. S2 S5) show  $50 \times 50 \mu\text{m}$  regions around the cropped selections here, and some earlier time points. Fig. 2a shows a cartoon with the typical pattern of movement, which was from the edge of the cell towards the centre. The unusually large degree of movement in sequence 2c is summarised by the spicule track in Fig. 2b. Sequence 2d is more typical of the extent of movement, with the spicules ending up on the region of the cell that would correspond to the high point of the discocyte as it lies flat, and also to the region with the lowest convex curvature. Sequence 2e again shows a large movement,

on a one of a kind example of a cell that had spontaneously distorted prior to the spicule movement. The distortion of the cell is shown in Fig. S4 of the supporting information, and is presumably due to an inhomogeneity of the adhesive layer. This cell appears to be stretched, unlike the other cells in these experiments. The rate of spicule movement in this sequence was up to  $2.7 \mu\text{m}/\text{min}$  (average  $0.94 \pm 0.12 \mu\text{m}/\text{min}$ ), similar to the rates for the sequence in Fig. 2c, but faster than that seen in sequence 2d, which was a relatively steady average velocity of  $0.1 \pm 0.01 \mu\text{m}/\text{min}$ . The spicule velocities for the cells in Fig. 2c, d and e are shown in the supporting information as Fig. S6.

The tracks for the spicules in sequence 2d are shown in Fig. S7. In contrast to the straight line path in Fig. 2b, the spicules follow a path seemingly closer to a random walk. The rms distance cannot be calculated with sufficient precision to determine if the spicules are moving at the rate that would be expected for diffusion. In contrast, the track of the spicule movement for sequence 2e is shown in the supporting information, as Fig. S8; as for the track in Fig. 2c, the path follows a straight line. The tilted cell in sequence 2f is of interest because it provides a different angle for viewing the spicule shape. The spicule appears to have a shape similar to that of the spicules that can be seen in profile at the rim or the cell.

### 3.2. Spicule splitting

In addition to the formation and movement of spicules, we also observed spicules that spontaneously split into daughter pairs. Fig. 3 shows three examples of cells with spicules that split apart. Criteria for identifying splitting events are that a second spicule appeared at the same time that an initially present spicule decreased in size. In the sequence in 3c, the second spicule moves away from an initially present spicule which remains at a fixed position, as shown in the track in Fig. 3b. The sequence in 3d shows two daughter spicules that move

away from each other, after which one undergoes a second split. The sequence in 3e appears to show an intermediate shape between the single spicule that was present up to 7.1 min, and the clearly defined pair that is present at 7.8 min, implying that the splitting event takes place over a period of some seconds.

### 3.3. RBC behaviour in high salt; ruffles vs. moving spicules

The sequences in Fig. 4 and Fig. 5a were acquired in high salt. A small volume of the cell suspension was added to the dips in the PAH coated slides and allowed to evaporate. Addition of PBS caused the cells to lyse, as illustrated in Fig. S11 of the supporting information; this implies that the salt concentration inside the cells has increased, making the PBS hypotonic to the cells under these conditions. Under these conditions, the cells formed ruffled edges but no individual spicules. The side view of the cells in Fig. 5 shows a comparison of the behaviour in high and isotonic salt: in high salt, it is clear that the cells have a continuous ruffled edge, while in isotonic buffer, the spicule that forms at the edge separates into daughter spicules that move towards opposite faces of the cell.

### 3.4. Reversibility and reproducibility of spicule formation

The top two rows of Fig. 6 show the reversibility of spicules that are formed in association with hypertonic buffer. Buffer tonicity was varied here by allowing the buffer to evaporate, leading to the echinocyte formation as seen in the top row of Fig. 6. Addition of more of the initial isotonic PBS diluted the medium in the well of the slide and reversed the process, as illustrated in the middle row of Fig. 6; continued evaporation from the open slide led to a second formation of the echinocyte, as shown in the bottom row of Fig. 6. The spicules formed reproducibly at the same positions, but in a different order.

Fig. S15 in the supporting information shows additional images

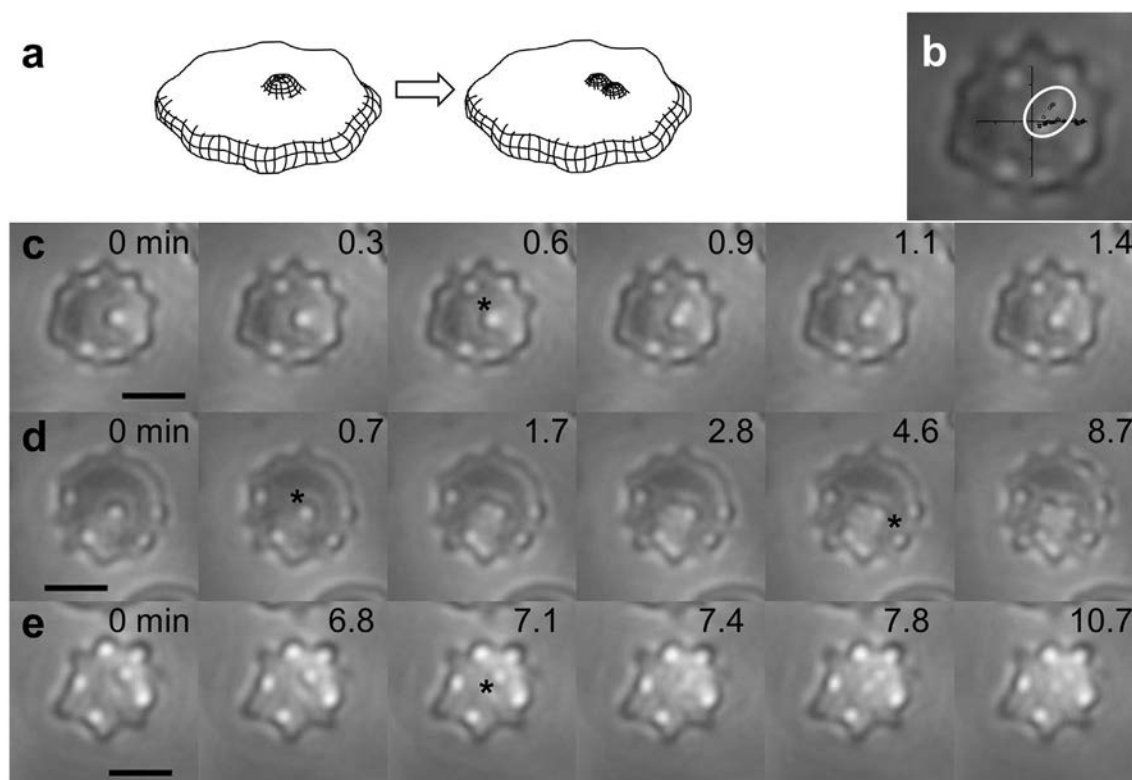


**Fig. 3.** Examples of spicules that split, as indicated in the cartoon in Fig. 3a. The track circled in 3b shows the movement of the daughter spicule that splits off from the spicule shown in Fig. 2b. The numbers show the time in minutes relative to the initial images and the scale bars show  $5 \mu\text{m}$ . Additional figures in the supporting information (Figs. S2, S9, S10) show  $50 \times 50 \mu\text{m}$  regions around the cropped selections here. Supporting information: video Fig. 2c 3c; video Fig. 3d; video Fig. 3e.

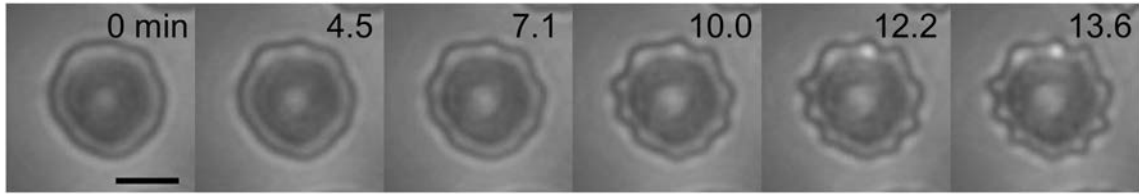


**Fig. 4.** Example of a cell forming a ruffled edge in high salt but no regular spicules. An additional figure in the supporting information (Fig. S12) shows a  $50 \times 50 \mu\text{m}$  region around the cropped selection here. The numbers show the time in minutes relative to the initial images and the scale bars show  $5 \mu\text{m}$ . Supporting information: video Fig. 4.

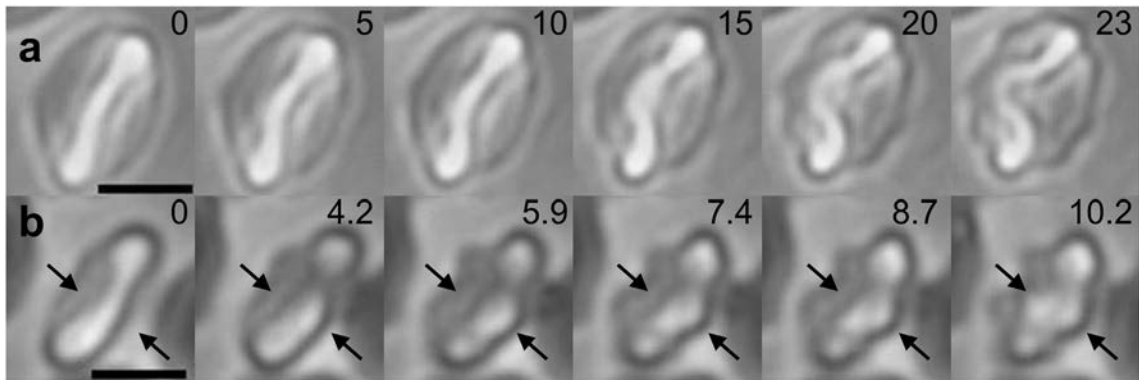


**Fig. 5.** Side views of cells, showing formation of a ruffled edge in high salt conditions (a, top), and formation of spicules (see arrows) after addition of a coverslip (b, bottom). The numbers show the time in minutes relative to the initial images and the scale bars show  $5 \mu\text{m}$ . Additional figures in the supporting information (Figs. S13 and S14) show a  $50 \times 50 \mu\text{m}$  region around the cropped selections here. Supporting information: video Fig. 5a; video Fig. 5b.

from the sequence in which the echinocyte reverses, from time points between 54 and 63 min; the spicule visible at 54 min remains constant until 62 min. Fig. S16 shows a  $50 \times 50 \mu\text{m}$  region around selected cropped selections. In this, it can be seen that there is a diversity of cell responses; some cells show little change in shape over the whole time course, while others undergo shape changes that are not reversed. In vivo, RBCs will circulate for about 120 days; at the time of collection, RBCs will have a range of ages, which can lead to diverse responses.

#### 4. Discussion

##### 4.1. Spicule behaviour: a summary

The question of interest is whether the results presented here demonstrate that there is lateral segregation in the RBC membrane during echinocyte formation, and, if so, whether that lateral segregation is associated with the cytoskeleton or with domains in the lipid bilayer.

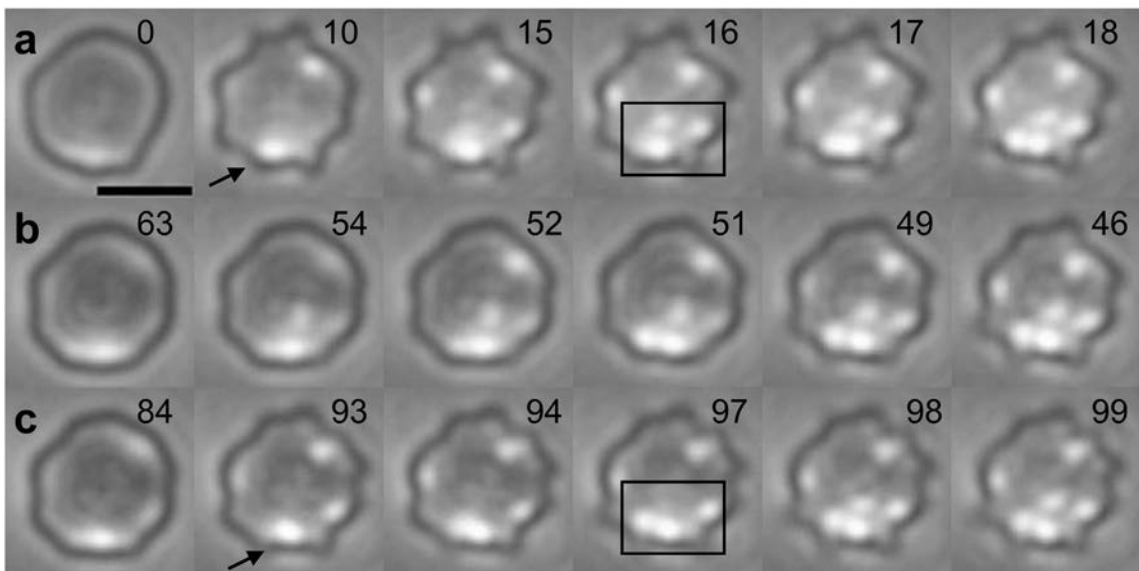


**Fig. 6.** Formation of spicules in an uncovered slide in association with evaporation of PBS (top row, a), followed by reversal of the process on addition of more PBS at 46 min (middle row, b; the images are shown in reverse order of acquisition, for comparison to rows a and c), and formation of spicules a second time as the evaporation continued (bottom row, c). The numbers show the time in minutes relative to the initial image and the scale bars show  $5 \mu\text{m}$ . The final positions of the spicules are similar both times the echinocyte shape is formed, as can be seen by comparing the images at 18 and 99 min. The differences in the sequences are highlighted by the arrows at min 10 and 93, which indicate a difference in curvature at the rim of the cell, and also by the boxed region at min 16 and 97, which shows differences in spicule formation at one point in the sequence. Supporting information: video Fig. 6.

**Table 1**

A summary of our observations about spicule behaviour, together with explanatory comments or implications with regards to the bilayer and the cytoskeleton.

Observation	Comment
Spicules form initially at rim of cells	Lower energetic barrier to spicule formation at rim due to geometry of cytoskeleton deformations [3]; lipid domains would be expected to form at rim, where Gaussian curvature is greatest [15–17]
Spicules can move (Fig. 2)	Lipid domains in model systems can move and fuse in vesicles [10,11,18,19]; lipid domain fusion in RBCs under tension [20] implies ability of domains in RBCs to move
Spicule movement is away from rim (Fig. 2, 5b)	Lipid domains can be specifically depleted on highly bent regions [21,22] but there is no obvious mechanism to drive the movement of a cytoskeletal deformation away from the energetic minimum at the rim
The most typical movement pattern is from rim to location corresponding approximately to the thickest point of the discocyte (Fig. 2d)	Typical movement is from the highly curved rim to the position of lowest convex curvature, which would be consistent domains moving away from more highly curved regions [21,22]
Spicule movement can approximate diffusion control (Fig. S7) but can also follow straight line (Figs. 2b, S8)	Diffusion control would be expected for domain diffusing in bilayer; directional control implies energy gradient associated with RBC shape or membrane inhomogeneity
Movement of the spicules stops at reproducible positions (Fig. 6)	Implies that the end location of spicules is affected by local features in the cytoskeleton
Spicules can split (Fig. 3)	With fixed conditions, lipid domains would be expected to fuse to minimise line tension, although multiple stable domains can exist on single vesicles [11]. Cytoskeleton-based models of RBCs can predict the numbers of echinocyte spicules but not dynamics of formation [9].
No spicule formation in high salt; ruffles formed instead (Fig. 4, 5a)	Increased rigidity of the cytoskeleton that has been reported in association with high salt [23,24] may prevent the formation of the circular spicules. Lowering the shear resistance of the cytoskeleton makes it easier for spicules to form in response to added lysolipids [25].
Spicules form in response to many factors [1,4,5]	If the spicules are associated with a single defined lipid composition that differs from the surroundings, then the relevant lipid(s) must be able to respond after RBC exposure to different echinocytic agents
Spicules remain when cell appears to be stretched (Fig. 2e)	Lipid domains on RBCs may disappear on stretching [25] or may coalesce [20]
Spicules have a curvature that differs from the surroundings	Lipid domains can sort by curvature [11,21,26]

The early stage spicules formed during echinocytosis have diameters of up to 2  $\mu\text{m}$ ; if they are associated with chemically distinct regions, this would then correspond to large scale lipid domains. The starting point of the discussion is a summary of the observations given in Table 1, together with comments comparing the observed behaviour to that noted elsewhere for lipid domains or for the cytoskeleton.

Spicule formation is always a balance of energetic contributions of the lipid bilayer and the cytoskeleton. Increasing area difference between the leaflets of the bilayer drives the membrane curvature; the cytoskeleton, which is attached to the bilayer at regular points, becomes distorted as the bilayer bends. The shape that the RBC reaches will be an energetic minimum that is determined by the area difference between the inner and outer leaflets of the lipid bilayer, the ability of the lipid bilayer to bend to accommodate this, and the resistance of the cytoskeleton to stretching and shear. If the area difference between the inner and outer leaflets increases, then this will lead to a new energy minimum shape, and the cell can change shape accordingly.

#### 4.2. Cytoskeleton contributions to spicule behaviour

If we look at the cytoskeleton contributions that are summarised in Table 1, the initial position of the spicule is determined by the cytoskeleton, which is more readily distorted at the rim of the cell [3], a result that can be obtained by considering a cytoskeleton with uniform mechanical properties and a surface that does not have a uniform curvature. The end position of the spicules may also be affected by the surface curvature (Fig. 2d). In the examples where greater spicule movement is seen, it is possible that the cells have lost the central dimple of the discocyte; this is certainly apparent in Fig. 2e, in which the cell stretches itself on the surface prior to the spicule movement. It is therefore possible that the predominant spicule movement pattern is from the region of greatest curvature at the rim to the region of least curvature at the thickest point of the cell. As the echinocytosis progresses, and the central dimple is lost, this driving force for localisation would disappear, leading to the observed result that the spicules become uniformly distributed in later stage echinocytes.

The results of Fig. 6 imply that the cell has a shape memory with regards to the spicule positions: after the cell is restored to the initial discocyte position, the echinocyte spicules form a second time at reproducible positions. Lipids within the bilayer are able to diffuse

laterally, so that features that remain at fixed positions can be attributed to the cytoskeleton. Shape memory has been observed previously in discocytes, with markers that are attached to the rim returning to the rim after the cell is distorted [27]. This effect may be due to the fact that the cytoskeleton is not, in fact, a uniform two dimensional regular mesh, but rather a less regular mesh [28,29] in which the rim region differs from the central region [29]. It has also been suggested that the echinocyte spicules are associated with localised cytoskeleton defects [30], one possible explanation for the results that we see here. Detailed analysis of the membrane surface has revealed dimples with a diameter of up to 500 nm and a depth of 100 nm [28]; if the spicule locations are determined by surface curvature details, perhaps this is sufficient to stop spicule movement.

If we consider the spicule movement, the initial and the end positions seem to be affected by the cytoskeleton, which can be explained through relatively straightforward mechanisms as described above. We then come to the question of how the spicule can move while retaining its well defined circular base. If the spicule is associated with a chemically distinct lipid domain, then the possibility of movement is easier to understand: the domains would be expected to be able to move within the fluid lipid bilayer. The direction of movement for the spicules is from the highly curved rim towards the regions with lower curvature. Small patches of lipids that separate would be expected to localise on the surface region with the highest Gauss curvature: this result has been found for ellipsoids [15,16], as well as for shapes more closely resembling discocytes, with regions of positive, zero and negative Gauss curvature [17]. For the RBCs, the region of highest Gauss curvature is on the rim, where the spicules are formed initially. These results would therefore support the initial formation of defined domains at the rim of the cell, but would not explain the movement of the spicules.

The depletion of lipid domains on curved surfaces has been observed previously in model systems [21,22]. In both these examples, domains with higher rigidity move to regions with lower curvature, suggesting that the bending energy of the membrane could contribute to the direction of domain movement.

Although lipid domains have the potential to move, the cytoskeleton is a fixed mesh: cytoskeleton driven spicule movement would not imply that a section of the cytoskeleton moves across the cell, but instead that a regular deformation moves across the cytoskeleton. We would have to

postulate a deformation that occurs initially at the energy minimum, and then reverses itself and moves away from the energy minimum position, something for which there is not an obvious mechanism. We may also note, in passing, that the spicules do not move around the rim, even if the cells maintain the early stage echinocyte shape (ellipsoidal with ripples around the rim) for an extended period of time.

We also demonstrate the spicule splitting events of Fig. 3. As mentioned above, the formation of echinocytes is associated with a change in the relative areas of the inner and outer leaflets, and it seems probable that the spicule splitting event is also driven by an increase in the area difference. If the spicules are associated with lipid domains, then the area difference could be localised rather than being evenly distributed over the cell surface; this would then provide a ready explanation for the localised splitting event. Lipid domains within a bilayer can certainly fuse, so the shape transition between a single spicule and a pair can be plausibly linked to the association of the spicules with lipid domains.

If we assume that the bilayer is uniform, we can then consider the spicule splitting event in terms of the cytoskeleton. It is possible to obtain an estimate of the total spicule number on the end stage echinocyte, based on the ratio of the bending to shear moduli for the membrane [9]. The mechanism by which the spicule numbers increase is not addressed by this model, but the transition to an increasingly spiculated state is expected to happen when the relative area difference between the leaflets passes a threshold value. If this is the case, then the sudden appearance of spicules would be expected, but it is not clear why a second spicule would form at a location that is already distorted, so that the cytoskeleton is already at increased energy relative to the unstressed areas with no spicules.

In summary, although we are unable to say that we have conclusive evidence for the existence of lipid domains on the spicules, our results can certainly be more readily explained if this is the case. A model of the possible events leading to the formation and movement of the spicules is given below, together with additional discussion of points listed in Table 1.

#### 4.3. Spicule splitting and membrane energy changes

As noted in Section 3.2, the spicule splitting proceeds as a spontaneous event. We can therefore consider the associated membrane energy changes and the possible factors driving the splitting process. Segregated lipid domains within a membrane have a line tension associated with the mismatch between the domain and the surrounding membrane [13]. The total line energy will then be a product of the line tension value and the boundary length. For the spicule splitting events, we have a well defined shape change: the spicule splits apart into two daughter spicules, which changes the boundary length, the curvature of the surface, and the relative areas of the inner and outer membrane leaflets, as illustrated in Fig. 7.

The boundary length associated with the spicules can be measured directly for top viewed spicules. The border of the bright region detected by phase contrast microscopy is assumed here to be the boundary at the base of the spicule. The spicule splitting proceeds spontaneously, indicating that it is energetically favourable; the increase in the line energy that would be associated with the increased boundary length must therefore be balanced by an energy decrease. The next step is therefore to consider the possible factors that could decrease the membrane energy.

The preferred (or relaxed) area difference  $\Delta A_0$  between the inner and outer membrane leaflets can change as a result of chemical changes to the cell membrane, leading to changes in the cell shape. The range of RBC morphologies from discocyte to echinocyte can be obtained as the minimum energy shapes for the varying values of  $\Delta A_0$  [2]. The effect of changing  $\Delta A_0$  is illustrated in Fig. 8 below: the membrane in its initial state (a) undergoes a chemical change that leads to state (b) with a new  $\Delta A_0$ ; this is then followed by the transition to state (c) as the cell

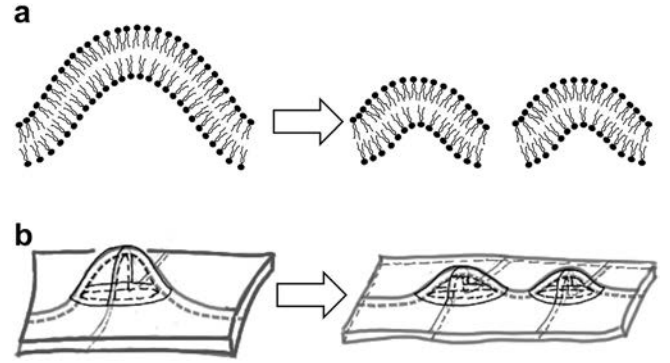


Fig. 7. The cell membrane has an inner and an outer leaflet, which are both affected as the spicules split (a; lipid molecules are not drawn to scale). The total circumference around the base of the spicules can change, along with the surface curvature (b). As the membrane becomes more highly curved, the area of the outer leaflet will increase relative to the area of the inner leaflet.

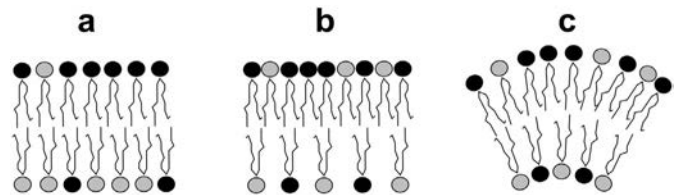


Fig. 8. Sequence of events associated with RBC shape changes. The membrane is initially in state (a). There is then a chemical change in the membrane, resulting in state (b), for example a reduction in ATP levels affecting the ATP-dependent systems that maintain lipid asymmetry. In response to the chemical changes, the membrane then changes shape, resulting in state (c). The change from (b) to (c) is associated with a change in cell shape and also with a decrease in membrane bending energy (see text).

morphology adjusts to a new minimum energy shape. In the transition from (a) to (b),  $\Delta A_0$  has changed, but the observed area difference  $\Delta A$  has not. The bending energy of the membrane is a function of the difference between the observed and preferred states, so that state (b) will be at a higher energy than (c). The change from (b) to (c) therefore represents a decrease in the membrane bending energy. The extent of this decrease can be estimated from observed changes in the membrane shape. For the spicule splitting events, these calculations are described in Appendix A. In terms of membrane physiology, the preferred area difference associated with the discocyte shape is the highest energy state, requiring continual energy in the form of ATP in order to maintain the required membrane asymmetry [31].

The changing curvature of the surface associated with the formation of smaller daughter spicules will affect both the cytoskeleton and the bilayer. Early stage echinocyte spicules with shapes similar to the spicules found here have been modeled using modified Gaussian functions. This leads to the result that the stress energy density associated with the cytoskeleton is highest around the boundary of the spicule, where the membrane surface bends away from the surrounding area [3]. For a fixed spicule height, increasing the boundary length would therefore be expected to contribute to an increase the energy associated with the cytoskeleton, which means that the energetic changes associated with the cytoskeleton are not driving the splitting event.

If spicules are modeled as regular ripples around the rim of the cell rather than as defined bumps with a circular base, doubling the number of spicules while decreasing the spicule height to 70% of the initial value (the number obtained if we assume a constant bilayer area for a hemisphere that splits into identical daughter hemispheres) would decrease the cytoskeletal energy [7]. This case, however, does not appear to be a good match to the shape changes in the spicule splitting events in Fig. 3, although it could apply to events such as that in Fig. 6

between minutes 16 and 17, showing spicule splitting at the rim of the cell.

The decrease in bilayer bending energy remains as the most likely possible driver for the spicule splitting events, after the line energy associated with the boundary and the energy associated with the cytoskeleton are both eliminated. The bilayer bending energy  $E_b$  includes a contribution from the intrinsic curvature and a second contribution from the area difference between the inner and outer leaflets. We can then compare this value to the change in line energy, done in Appendix A by calculating a line tension value that would be associated with the observed change in  $\Delta A$ , together with the energy associated with the cytoskeleton.

#### 4.4. Lipid domains, the echinocyte spicules and cholesterol

Red blood cells have been studied extensively: the lipid composition has been analysed [32–34], phase diagrams have been prepared for model systems [35–37], and whole red blood cells and RBC ghosts have been characterized using fluorescent markers, atomic force microscopy and other techniques. It is well established that the RBC membranes are not homogeneous, and that lateral segregation exists on at least some length scale: Fourier transform infra red spectroscopy has identified membrane phase transitions indicative of domain formation [38,39]; fluorescence studies have shown RBC membranes to be more ordered around the cell perimeter [40]; fluorescent markers have been used to identify localised lipid domains [20,41–49]. Lateral segregation of lipids in the RBC membrane has been identified in discocytes that are native, apart from added fluorophores [20,41,43–45,48,49], and in response to added calcium [31], cell deformation [43], toxins that affect the cells or induce the formation of echinocytes [42,50] and after storage to age the cells [43]. Membrane proteins may have an important role in the stabilisation of any lipid domains: regions identified by lipid specific markers have been found to correspond to lateral segregation of mobile membrane proteins [46], domains have been shown to be linked to the cytoskeleton [41], and domains identified in intact membranes have been found to be not present in vesicles prepared from membrane lipids [45].

Cholesterol makes up 40–45% of the lipid portion of the RBC membrane, with sphingomyelin making up about 25% of the phospholipids [32,33]; palmitoylcholine (POPC) is one of the single most common phosphatidylcholines [32]. Ternary phase diagrams for cholesterol, sphingomyelin and POPC show that at 40% cholesterol and 15% sphingomyelin, phase separation into liquid ordered and liquid disordered domains may occur [35]. Other work has suggested that only one phase will be present at this particular composition [36], so that the phase separation observed in vesicles prepared from whole cell membranes may be associated with the interactions between membrane lipids and membrane proteins [51]. An additional point to consider is that the RBCs in the experiments presented here were all cooled prior to use, which can result in phase separated regions that are not at a thermodynamic equilibrium [52].

Phospholipids have an asymmetric distribution between the inner and outer leaflets of the membrane, actively maintained by ATP dependent enzymes [33,53]. As RBCs age during storage, the decreasing ATP content of RBCs affects the cell shape [4], possibly by affecting the ATP dependent transport systems [53]. Lipids that are predominantly in the inner leaflet appear in the outer leaflet as the cells age: one example of this is phosphatidylserine (PS), which appears externally in increasing amounts during ageing of RBCs [54]. Due to the correlation between PS appearance and RBC ageing, PS has been a candidate for association with the spicule formation; however, large scale PS domains that have been identified on RBCs using fluorescent labels do not localise on the spicules [42].

Unlike phospholipids, cholesterol can flip flop readily between the lipid leaflets in the absence of an active transport system, because the small size of the hydroxyl head group leads to a relatively low energy

barrier for movement through the hydrophobic bilayer [34]. Cholesterol would therefore meet the criterion listed in Table 1, in that it could respond readily to different echinocytic agents: it would be able to flip between leaflets, in addition to lateral movement. There is little agreement about the distribution of cholesterol between the inner and outer leaflets of RBCs, with measured values from different experiments showing an excess in either the outer or the inner leaflets, as well as others suggesting equal concentrations [34]. Cholesterol is associated with strongly curved regions due to its shape and small hydrophilic head group [11]; in addition, its rigid ring structure can affect the bilayer mechanical properties, increasing the bending modulus [55].

In model systems, cholesterol rich domains have demonstrated a variety of interesting behaviours: in supported bilayers, they have been shown to sort by substrate curvature, becoming depleted on curved regions [21]; they have also been shown to undergo spontaneous out of plane budding after reaching a sufficiently large size, followed by expulsion of the cholesterol rich liquid ordered domains from the highly curved region [22]. In a system with a mixed continuous mono and bilayer, the cholesterol rich domains have been shown to form preferentially in the monolayer regions of system [56], which serves as a reminder that the typical assumption of bilayer symmetry during modeling is not necessarily valid. Cholesterol distributes asymmetrically in the leaflets of bilayer vesicles, although the technique used to measure this was unable to determine whether the inner or the outer leaflet had the higher cholesterol concentration [57].

In RBCs, large scale domains enriched with cholesterol have been identified using fluorescent markers [43,44] and have been found to be associated with regions having induced convex curvature, or that are forming vesicles [43]. Exposure of RBCs to cholesterol attached to poly (ethylene glycol) (PEG) so that it remained confined to the outer leaflet produced echinocytes in which the labeled cholesterol PEG was shown to be localised on the spicules [58]. Cholesterol by itself would tend to impart a negative rather than a positive curvature due to the small size of the hydrophilic head group, but an asymmetric distribution with an excess in the outer leaflet could be associated with the observed effect. Measuring the relative amounts of cholesterol in the inner and outer leaflets of RBC membranes has produced a wide range of results (reviewed in [34]).

Additional evidence for the segregation of lipids on the echinocyte spicules comes from the fact that vesicles that are shed from the ends of the spicules after the spicules elongate have been shown to have a lipid composition that differs from the whole cell [59], and also to include proteins associated with lipid rafts [60], which would be consistent with the enrichment of cholesterol and sphingomyelin on the spicules.

Removal of cholesterol from RBCs results in a shape change opposite to the effect seen with echinocyte formation: the cells form stomatocytes, [61–63], cup shaped cell forms associated with the expansion of the inner membrane leaflet relative to the outer leaflet [2]. This effect is, however, not straightforward, and is probably due to a complex combination of effects that membrane cholesterol content has on the membrane bound enzymes [63].

#### 4.5. Line tension values

The spicule splitting events were used to estimate an upper range for line tension value of approximately 0.4 pN in association with the putative lipid domains localised on the spicules, as described in Appendix A. The calculations are based on the assumption that the decrease in membrane bending energy is sufficient to counteract the increase in membrane energy associated with the increased domain boundary length as the spicules split. Fig. 8 shows how the increased curvature on splitting is associated with a decrease in membrane bending energy. The calculations are a simplification that do not include consideration of the cytoskeletal contribution. This would mean that we are calculating an upper limit for the line tension, not including other possible factors that could affect the calculated value. This does, however,

provide a value that can be compared to other reported line tension values, and a procedure that could be applied in future and more detailed analyses.

Values for line tension have been measured for monolayers and bilayers of different compositions, and have also been estimated theoretically. The theoretical calculations suggest a value as high as 10 pN [64]. The expected value will depend on the height mismatch between lipids at the domain boundary [13], and will be reduced if one component of the system can adsorb to the boundary line [64]; it will also drop to 0 as the pressure increases to the critical point at which the domains merge. A theoretical consideration of the kinetics of lipid domain growth has suggested that a line tension of 0.4 pN is sufficient to drive the formation of micrometre scale domains [65]. Line tension values of 0.67 [66] and 1.2 pN [67] have been reported for systems with phospholipid, sphingomyelin and cholesterol, similar to values reported for other lipids [68]. We can therefore see that the values in Table A1 are consistent with both theoretical and measured values given elsewhere.

Numerous factors other than the cytoskeletal contributions could affect the calculated line tension value, starting with the fact that our calculation is proportional to the bilayer bending modulus, and is therefore reliant on values that have been measured elsewhere [55,69–74]. Additional shape changes in the cell distal from the splitting spicules were not considered, which could have resulted in an underestimation of the area difference energy stored in the membrane prior to the split; we also assume that a fixed change in the area difference between the membrane leaflets corresponds directly to an observed shape change. This will not necessarily be true: calculations including the curvature preference, the relative area difference and an assumed shape for the spicules have suggested previously that there are relatively broad energy minima that would allow RBCs to retain their shape as the relative area difference changes, until threshold values are reached [69].

#### 4.6. A model for events during spicule formation

One possible model for the sequence of events that occur during the formation and movement of spicules is as follows; some of the listed points are well established, as indicated by the cited references, and some are speculation. The lipid composition of the RBC membrane allows the formation of liquid ordered domains [35]; in whole cells, separate domains have been noted under multiple conditions [20,38–49]. Larger scale domains enriched in cholesterol may form, possibly at fixed positions but with mobility of the individual cholesterol molecules [44]. If the RBCs age during storage [4], or if they are exposed to other echinocytic agents [5], the outer leaflet of the membrane expands relative to the inner leaflet. The increasing difference in the relative areas of the inner and outer leaflets drives the formation of convex bumps [1,2]; these form initially at the rim of the cell, due to energetic considerations relating to the geometry of the cytoskeleton deformations [3]. The changing surface curvature at the rim of the cell may allow nanoscale lipid domains to sort by curvature [26]; additionally, the cholesterol in the membrane can flip flop readily between leaflets [34], which could form domains with an asymmetric distribution of cholesterol, and a membrane region with an intrinsic curvature. In order to form spicules with a circular base, the lipid associated curvature and bending driven by the line tension would have to overcome the resistance of the cytoskeleton; if the cytoskeleton is too rigid, as appears to be the case in the high salt conditions of Fig. 4 and 5a [24], then the

## Appendix A

### A.1. Calculations relating to line tension

The spicule splitting proceeds as a spontaneous event, so that it can be seen that the overall membrane energy changes are negative. The increase in boundary length on splitting will lead to an increase in line energy; this must therefore be balanced by a decrease in other aspects of the membrane

RBCs form a ruffled edge rather than separate spicules, a pattern that is also seen under some conditions for cells from species with a higher ratio of protein to lipid than in human RBCs [75]. Cholesterol enriched domains would have a higher bending modulus [55], and could, possibly because of the increasing size of the relatively rigid domain, move away from the highly curved rim, a pattern that has been seen in model systems [21,22]. The spicules in this suggestion would be curved but rigid, so that individual spicules of sufficient size would have to distort in order to be accommodated on the rim, and would therefore move to region that would provide a flatter base. This would produce the cholesterol enriched spicules of the early stage echinocyte, as identified by specific labels [43,58]. The spicule movement directed by the curvature of the underlying surface could then be stopped by changing curvature associated with dimples, which are known to occur on the RBC surface [28]. Increasing area difference between the leaflets would then increase the number of spicules on the surface [76], in some cases as seen here by splitting existing spicules.

### 4.7. Conclusions

The spicule behaviour in the early stages of the echinocyte formation can be explained more readily if the spicules are associated with the lipid domains that have been identified elsewhere as being associated with the spicules [43,58]. The observations presented here have been made under label free conditions, supporting the idea that large scale lipid domains can exist in cells without the presence of a label. The reproducibility of the spicule positions after the echinocyte formation is reversed suggests that there are also heterogeneities in the cytoskeleton, and that these can affect the spicules position. We also demonstrate an approach to measuring line tension in early stage echinocytes, based on well defined shape changes that occur in RBCs as the echinocyte spicules spontaneously split.

### Author contributions

KAM designed and carried out experiments and wrote the paper; KAM and SMF did the calculations; SMF analysed images and prepared computing algorithms; KB provided samples and arranged ethics vote. All authors read the manuscript and contributed towards the final draft.

### Funding

This work was supported by the German Research Foundation DFG [KAM: ME 4648/2 1; KB: BI 1308/5 1].

### Declaration of competing interest

The authors declare that they have no known competing financial interests or personal relationships that could have appeared to influence the work reported in this paper.

### Acknowledgements

The authors thank the blood donors of Baden Württemberg Hessen.

energy. As illustrated in Fig. 8, the increase in bending is a response to chemical changes in the cell membrane and represents a relaxation to a lower energy state. In other words, the contribution associated with the bending energy is negative. We can estimate the extent of this contribution from the known shape changes that occur as spicules split apart into daughter pairs. The line tension is estimated here by equating the absolute value of the line energy change with the absolute value of the bending energy change, or  $\Delta E_{\text{line}} = \Delta E_b$ , written here without the notation for absolute value. Since this calculation ignores the cytoskeletal and other contributions to the membrane bending energy, we are only estimating a possible upper limit to the line tension.

Part 1 of the calculation procedure is to determine the boundary lengths of the spicules before and after the splitting events. This was done as described in Section 2.6 of the Materials and Methods; results are summarised in Table A1.

Part 2 is to determine the spicule profiles. Since the spicules are viewed directly from above, this can only be estimated. We follow two different procedures: in one (summarised as procedure a in Table A1), we treat the spicules as if they are hemispheres, and in the second (procedure b) we assume that the spicules on the top surface of the cell have the same shape as the spicules that can be seen in profile.

For calculation b, the shape of top view spicules was assumed to be axisymmetric and characterized by a shape function,  $z(r)$  of the form [3]:

$$z(r) = h \cdot \exp\left[-\frac{A^2}{(R_b - r)^2}\right] \cdot \exp\left[-\left(\frac{r}{c}\right)^\alpha\right] \quad (\text{A1})$$

where  $R_b$  and  $h$  are, respectively, the spicule radius at its base and the spicule height at its centre. The coordinate  $r$  is the distance from the centre of the spicule to the spicule edge, and  $A$ ,  $c$  and  $\alpha$  are shape parameters.

These shape parameters were assumed to be constant and equal to the average values of those obtained for edge spicules, according to the following procedure:  $(x,y)$  profiles of edge spicules were obtained from spline curves of cell contours, which were in turn determined by the same procedure described above. These data sets were then converted into  $(r,z)$  profiles by rotating the axes and shifting the origin of the coordinate system to the centre of the spicule base. The profiles were then divided with respect to the symmetry axis, for each of which shape parameters were determined from best (NLSF) fits to the shape function. The average values of the fitting parameters for 14 such half profiles were as follows:  $A$ :  $0.30 \pm 0.05$ ;  $\alpha$ :  $2.08 \pm 0.07$ ;  $c$ :  $0.75 \pm 0.07$ ; all values in  $\mu\text{m}$ ;  $h/R_b$ :  $0.80 \pm 0.09$ . The  $R_b$  values were obtained from boundary lengths by calculating the radius of a circle with equivalent circumference.

Part 3 of the calculation is then to estimate the energy difference associated with the change in bending during the spicule splitting. The initial calculation (a) is based on a simplified version of expression for  $E_b$  given by the area difference elasticity or ADE model in Eq. (A2) [2,3]. In this expression, the first term arises from the difference between the sum of the principal curvatures (twice the mean curvature, or  $2H$ ) and the preferred curvature  $C_0$  of the spicule surface  $S$ ;  $\kappa$  is the local bending modulus. The second term is due to the non local curvature, which arises from the relative area difference of the inner and outer leaflets [69]. There is an energetic penalty if the actual area difference between the leaflets is not equal to the preferred area difference: in this term,  $A$  is the area,  $\kappa_A$  is the non local bending constant, and  $D$  is the separation distance between the leaflets.

$$E_b = \frac{\kappa}{2} \int_S (2H - C_0)^2 dS + \frac{\kappa_A \pi}{AD^2} (\Delta A - \Delta A_0)^2 \quad (\text{A2})$$

The change in membrane bending energy is attributed entirely to the change in the area difference, so that the absolute value of  $\Delta E_b = ((\kappa_A \pi) / (AD^2)) (\Delta A_{\text{split}})^2$ , where  $\kappa_A = \kappa / \pi$  [2,3]; we also assume that the spicule area  $A$  is the area of the initial parent spicule;  $D$  is the separation distance between the membrane leaflets, and  $\Delta A_{\text{split}}$  is the change in the relative areas of the inner and outer leaflets assuming a separation distance  $D$  and hemispherical spicule shapes. We use a bending modulus value of  $1 \times 10^{-19}$  J, discussed below in the section on assumptions and limitations in the calculations. Calculations were done in a stepwise fashion using a value of 3 nm for the separation distance  $D$  [3], but this value is eliminated in a general mathematical derivation and therefore does not affect the results.

In the second procedure employed here for calculating the line tension (calculation b), we assume that the preferred curvature  $C_0$  is 0, leading to Eq. (A3). This assumption would not be valid for RBC membranes because of the asymmetry between the membrane leaflets, but we face the limitation that the preferred curvature  $C_0$  is an unknown value, and we therefore employ this as an approximation. As for the calculation procedure a, it can be shown that this value does not affect the final outcome of the calculations.

$$E_b = \frac{\kappa}{2} \int_S (2H)^2 dS + \frac{\kappa_A \pi}{AD^2} (\Delta A - \Delta A_0)^2 \quad (\text{A3})$$

The spicule's mean curvature as a function of  $r$  was determined from the first and second fundamental forms [3] and the shape function  $z(r)$  in polar coordinates according to the expression:

$$2H = \frac{d^2 z}{dr^2} \cdot \frac{1}{\left[\left(\frac{dz}{dr}\right)^2 + 1\right]^{3/2}} + \frac{1}{r} \cdot \frac{dz}{dr} \cdot \frac{1}{\left[\left(\frac{dz}{dr}\right)^2 + 1\right]^{1/2}} \quad (\text{A4})$$

where the first and second derivatives of  $z(r)$  were the analytically calculated from the shape function given above. The area difference of the spicule was calculated from the mean curvature as follows [3]:

$$\Delta A = D \cdot \int_S 2H \cdot dS = D \cdot \int_0^{r \geq R_b} 2H \cdot r \cdot \left[\left(\frac{dz}{dr}\right)^2 + 1\right]^{1/2} dr \quad (\text{A5})$$

Table A1 summarises the calculations made using the two different approaches described above, both of which assume that  $\Delta E_{\text{line}} = -\Delta E_b$ . Results from both calculation procedures are similar for all three splitting events, ranging from 0.22 to 0.66 pN. The average of all the line tension values in Table A1 is  $0.41 \pm 0.05$  pN (standard error of the average).

Table A1

Changes in measured and calculated values associated with spicule splitting events, assuming that  $\kappa_A = 1 \times 10^{-19} \text{ J}$ . Calculation (a) uses  $\Delta E_{\text{line}} = ((\kappa_A \pi)/(AD^2)) (\Delta A_{\text{split}})^2$  and assumes hemispherical spicules; calculation (b) includes a term for the intrinsic curvature as described above and assumes that the spicules conform to the shape function in Eq. (A1).

Splitting event and associated images	Boundary length before split ( $\mu\text{m}$ )	Total boundary length after split ( $\mu\text{m}$ )	Line tension calculation a (pN)	Line tension calculation b (pN)
Fig. 3c between 0.6 and 0.9 min	6.7	11.9	0.29	0.39
Fig. 3d between 0.7 and 1.7 min	6.1	9.3	0.22	0.66
Fig. 3d between 4.6 and 8.7 min	4.7	8.5	0.42	0.51
Fig. 3e between 7.1 and 7.8 min	6.2	10.5	0.28	0.49

## A.2. Assumptions and limitations in the calculations

In the calculations, we have used a value of  $1 \times 10^{-19} \text{ J}$  for the local bending modulus  $\kappa$ . The non local bending constant  $\kappa_A$  in Eq. (A2) and in calculations a and b of Table A1 is assumed here to be related to  $\kappa$  according to  $\kappa_A = \kappa/\pi$ , following calculations used elsewhere [2, 3; note that  $\kappa_A$  is defined differently, but the expressions for the bending energy also differ, so that the calculations are equivalent). The non local bending modulus refers to the redistribution of the lipid density in the inner and outer leaflets of the RBC membrane. Ratios other than the one used here have been assumed elsewhere, but this may be due to the associated experiments, in which membrane tethers were drawn out from the RBCs and the value for the non local bending constant was attributed to the difference in material that is drawn up from the inner and outer leaflets [70]. Literature values for the bending modulus  $\kappa$  range from  $0.2 \times 10^{-19} \text{ J}$  to  $9 \times 10^{-19} \text{ J}$  [55,69–74]. The value that we calculate is directly proportional to the bending modulus, giving us an associated wide range of possible values. The local bending contribution to the membrane energy has some effect on our calculations, as seen by the difference between the line tension energies calculated by the two different procedures used here, but this difference is relatively minor compared to the other possible factors listed here.

As mentioned, we did not include the cytoskeletal contributions to the energetic changes associated with the spicule splitting events, so that we are effectively estimating a limiting value, where  $|\Delta E_{\text{line}}| \leq |\Delta E_b|$ . The resistance of the membrane to changes in bending has been attributed mostly to the lipid bilayer [77], but the cytoskeleton appears to become significant under some conditions.

The spicule splitting events are accompanied by other changes to the cell shape, which are not taken into account during the calculations. Some changes may be seen on close inspection; for example, in sequence 3d, the spicule at the 6 o'clock position becomes more curved between the 0.7 and 1.7 min time points that bracket the spicule splitting. The stored energy in the membrane prior to the splitting event therefore appears to be greater than the value calculated from the area difference term, which would lead to underestimation of the line tension value.

It is possible to calculate the energetic contributions of the cytoskeleton for single spicules [3], but this is based on the assumption that the membrane has uniform properties. One limitation here is that the cytoskeleton itself is not uniform [27,29], a fact that should be considered when explicitly investigating the movement of spicules across the RBC surface. A second limitation is that the shape at the spicule boundary, in the region that contributes most strongly to the cytoskeleton energy, is unknown: if the lipids do separate into domains associated with the spicules, then the shape at the domain boundary will be determined by the relative values of the bending moduli for the two different compositions [66]. More precisely, the shape at the neck between two separated phases would be determined by the differences in the Gauss moduli that describe the response to changes in the Gaussian curvature [66] (the Gaussian curvature is intrinsic to the surface; a flat surface can be wrapped around a cylinder, and thus the flat surface and the cylinder have the same Gaussian curvature).

A more complete treatment of the spicule splitting events could include a term for the Gaussian curvature, which may be relevant, due to the fact that we are considering events in which the Gaussian curvature changes, plus we make calculations for a region with a defined boundary [78]; terms relating to the demixing could be included, since the distribution of the lipids will contribute to the membrane energetics [79]; it would also be possible to consider local changes to the intrinsic curvature, if the cholesterol has an asymmetric distribution in areas of specific curvature. In summary, if we have an irregular surface with changing curvature and multiple components, it would be challenging to calculate all aspects of the membrane energy [79].

## References

- [1] M.P. Sheetz, S.J. Singer, Biological membranes as bilayer couples- molecular mechanism of drug-erythrocyte interactions, *Proc. Natl. Acad. Sci. U. S. A.* 71 (1974) 4457–4461, <https://doi.org/10.1073/pnas.71.11.4457>.
- [2] G. Lim, M. Wortis, R. Mukhopadhyay, Stomatocyte–discocyte–echinocyte sequence of the human red blood cell: evidence for the bilayer– couple hypothesis from membrane mechanics, *Proc. Natl. Acad. Sci. U. S. A.* 99 (2002) 16766–16769, <https://doi.org/10.1073/pnas.202617299>.
- [3] G.R. Lazaro, K.A. Melzak, J.L. Toca-Herrera, I. Pagonabarraga, A. Hernandez-Machado, Elastic energies and morphologies of the first stages of the disc-cochocytocyte transition, *Soft Matter* 9 (2013) 6430–6441, <https://doi.org/10.1039/c3sm50716e>.
- [4] M. Nakao, T. Nakao, S. Yamazoe, Adenosine triphosphate and maintenance of shape of the human red cells, *Nature* 187 (1960) 945–946, <https://doi.org/10.1038/187945a0>.
- [5] P. Wong, A basis of echinocytosis and stomatocytosis in the disc-sphere transformations of the erythrocyte, *J. Theor. Biol.* 196 (1999) 343–361, <https://doi.org/10.1006/jtbi.1998.0845>.
- [6] H.J. Deuling, W. Helfrich, Red blood cell shapes as explained on the basis of curvature elasticity, *Biophys. J.* 16 (1976) 861–868.
- [7] K.A. Melzak, G.R. Lazaro, A. Hernandez-Machado, I. Pagonabarraga, J.M. Cardenas Diaz de Espada, J.L. Toca-Herrera, AFM measurements and lipid rearrangements: evidence from red blood cell shape changes, *Soft Matter* 8 (2012) 7716–7726, <https://doi.org/10.1039/c2sm25530h>.
- [8] K. Khairi, J. Foo, J. Howard, Shapes of red blood cells: comparison of 3D confocal images with the bilayer-couple model, *Cell. Mol. Bioeng.* 1 (2008) 173–181, <https://doi.org/10.1007/s12195-008-0019-5>.
- [9] R. Mukhopadhyay, H.W. G. Lim, M. Wortis, Echinocyte shapes: bending, stretching, and shear determine spicule shape and bending, *Biophys. J.* 82 (2002) 1756–1772, [https://doi.org/10.1016/S0006-3495\(02\)75527-6](https://doi.org/10.1016/S0006-3495(02)75527-6).
- [10] S.L. Veatch, S.L. Keller, Separation of liquid phases in giant vesicles of ternary mixtures of phospholipids and cholesterol, *Biophys. J.* 85 (2003) 3074–3083, [https://doi.org/10.1016/S0006-3495\(03\)74726-2](https://doi.org/10.1016/S0006-3495(03)74726-2).
- [11] T. Baumgart, S.T. Hess, W.W. Webb, Imaging coexisting fluid domains in biomembrane models coupling curvature and line tension, *Nature* 425 (2003) 821–824, <https://doi.org/10.1038/nature02013>.
- [12] F. Jülicher, R. Lipowsky, Shape transformations of vesicles with intramembrane domains, *Phys. Rev. E* 53 (1996) 2670–2683, <https://doi.org/10.1103/PhysRevE.53.2670>.
- [13] P.I. Kuzmin, S.A. Akimov, Y.A. Chizmadzhev, J. Zimmerberg, F.S. Cohen, Line tension and interaction energies of membrane rafts calculated from lipid splay and tilt, *Biophys. J.* 88 (2005) 1120–1133, <https://doi.org/10.1529/biophysj.104.048223>.
- [14] K.A. Melzak, S. Uhlrig, F. Kirschhöfer, G. Brenner-Weiss, K. Bieback, The blood bag plasticizer di-2-ethylhexylphthalate causes red blood cells to form stomatocytes, possibly by inducing lipid flip-flop, *Transfus. Med. Hemother.* 45 (2018) 413–422, <https://doi.org/10.1159/000490502>.
- [15] F.E. Baginski, R. Croce, S. Gillmor, R. Krause, Numerical investigations of the role of curvature in strong segregation problems on a given surface, *Appl. Math. Comput.* 227 (2014) 399–411, <https://doi.org/10.1016/j.amc.2013.11.008>.

- [16] S. Gillmor, J. Lee, X. Ren, The role of Gauss curvature in a membrane phase separation problem, *Physica D* 240 (2011) 1913–1927, <https://doi.org/10.1016/j.physd.2011.09.002>.
- [17] M.C. Barg, A.J. Mangum, A phase separation problem and geodesic disks on Cassinian oval surfaces, *App. Math. Comput.* 354 (2019) 192–205, <https://doi.org/10.1016/j.amc.2019.02.037>.
- [18] A. Roux, D. Cuvelier, P. Nassoy, J. Prost, P. Bassereau, B. Goud, Role of curvature and phase transition in lipid sorting and fission of membrane tubules, *EMBO J.* 24 (2005) 1537–1545, <https://doi.org/10.1038/sj.emboj.7600631>.
- [19] P. Cicuta, S.L. Keller, S.L. Veatch, Diffusion of liquid domains in lipid bilayer membranes, *J. Phys. Chem. B* 111 (2007) 3328–3331, <https://doi.org/10.1021/jp0702088>.
- [20] D. Tyteca, L. D'Auria, P. Van Der Smissen, T. Medts, S. Carpentier, J.C. Monbaliu, P. de Diesbach, P.J. Courtroy, Three unrelated sphingomyelin analogs spontaneously cluster into plasma membrane micrometric domains, *Biochim. Biophys. Acta* 1798 (2010) 909–927, <https://doi.org/10.1016/j.bbame.2010.01.021>.
- [21] M.I. Hoopes, R. Faller, M.L. Longo, Lipid domain depletion at small localized bends imposed by a step geometry, *Langmuir* 27 (2011) 2783–2788, <https://doi.org/10.1021/la104504p>.
- [22] Y.-S. Ryu, D. Yoo, N.J. Wittenberg, L.R. Jordan, S.-D. Lee, A.N. Parikh, S.-H. Oh, Lipid membrane deformation accompanied by disk-to-ring shape transition of cholesterol-rich domains, *J. Am. Chem. Soc.* 137 (2015) 8692–8695, <https://doi.org/10.1021/jacs.5b04559>.
- [23] K. Svoboda, C.F. Schmidt, D. Branton, S.M. Block, Conformation and elasticity of the isolated red blood cell membrane skeleton, *Biophys. J.* 63 (1992) 784–793, [https://doi.org/10.1016/S0006-3495\(92\)81644-2](https://doi.org/10.1016/S0006-3495(92)81644-2).
- [24] G. Lenormand, S. Hénon, A. Richert, J. Siméon, F. Gallet, Direct measurement of the area expansion and shear moduli of the human red blood cell membrane skeleton, *Biophys. J.* 81 (2001) 43–56, [https://doi.org/10.1016/S0006-3495\(01\)75678-0](https://doi.org/10.1016/S0006-3495(01)75678-0).
- [25] J.K. Khodadad, R.E. Waugh, J.L. Podolski, R. Josephs, T.L. Steck, Remodeling the shape of the skeleton in the intact red cell, *Biophys. J.* 70 (1996) 1036–1044, [https://doi.org/10.1016/S0006-3495\(96\)79649-2](https://doi.org/10.1016/S0006-3495(96)79649-2).
- [26] A. Tian, T. Baumgart, Sorting of lipids and proteins in membrane curvature gradients, *Biophys. J.* 96 (2009) 2676–2688, <https://doi.org/10.1016/j.bpj.2008.11.067>.
- [27] T.M. Fischer, Shape memory of human red blood cells, *Biophys. J.* 86 (2004) 3304–3313, [https://doi.org/10.1016/S0006-3495\(04\)74378-7](https://doi.org/10.1016/S0006-3495(04)74378-7).
- [28] R. Nowakowski, P. Luckham, P. Winlove, Imaging erythrocytes under physiological conditions by atomic force microscopy, *Biochim. Biophys. Acta* 1514 (2001) 170–176, [https://doi.org/10.1016/S0005-2736\(01\)00365-0](https://doi.org/10.1016/S0005-2736(01)00365-0).
- [29] A. Nans, N. Mohandas, D.L. Stokes, Native ultrastructure of the red cell cytoskeleton by cryo-electron tomography, *Biophys. J.* 101 (2011) 2341–2350, <https://doi.org/10.1016/j.bpj.2011.09.050>.
- [30] N.S. Gov, S.A. Safran, Red blood cell membrane fluctuations and shape controlled by ATP-induced cytoskeletal defects, *Biophys. J.* 88 (2005) 1859–1874, <https://doi.org/10.1529/biophysj.104.045328>.
- [31] D.M. Haverstick, M. Glaser, Visualization of Ca<sup>2+</sup>-induced phospholipid domains, *Proc. Natl. Acad. Sci. U. S. A.* 84 (1987) 4475–4479, <https://doi.org/10.1073/pnas.84.13.4475>.
- [32] J.T. Dodge, G.B. Phillips, Composition of phospholipids and of phospholipid fatty acids and aldehyde in human red cells, *J. Lipid Res.* 8 (1967) 667–675.
- [33] A. Zachowski, Phospholipids in animal eukaryotic membranes: transverse asymmetry and movement, *Biochem. J.* 294 (1993) 1–14.
- [34] T.L. Steck, Y. Lange, Transverse Distribution of Plasma Membrane Bilayer Cholesterol: Picking Sides, 19 (2018), pp. 750–760, <https://doi.org/10.1111/tra.12586>.
- [35] R.F.M. de Almeida, A. Fedorov, M. Prieto, Sphingomyelin/phosphatidylcholine/cholesterol phase diagram: boundaries and composition of lipid rafts, *Biophys. J.* 85 (2003) 2406–2416, [https://doi.org/10.1016/S0006-3495\(03\)74664-5](https://doi.org/10.1016/S0006-3495(03)74664-5).
- [36] R.S. Petruzielo, F.A. Heberle, P. Drazba, J. Katsaras, G.W. Feigenson, Phase behavior and domain size in sphingomyelin-containing lipid bilayers, *Biochim. Biophys. Acta* 1828 (2013) 1302–1313, <https://doi.org/10.1016/j.bbame.2013.01.007>.
- [37] T.M. Konyakhina, G.W. Feigenson, Phase diagram of a polyunsaturated lipid mixture: brain sphingomyelin/1-stearoyl-2-docosahexaenoyl-sn-glycerol-3-phosphocholine/cholesterol, *Biochim. Biophys. Acta* 1858 (2016) 153–161, <https://doi.org/10.1016/j.bbame.2015.10.016>.
- [38] W.F. Walkers, L.M. Crowe, N.M. Tsvetkova, F. Tablin, J.H. Crowe, In situ assessment of erythrocyte membrane properties during cold storage, *Mol. Mem. Biol.* 19 (2002) 59–65, <https://doi.org/10.1080/09687680110103613>.
- [39] R. Mendelsohn, D.J. Moore, Vibrational spectroscopic studies of lipid domains in biomembranes and model systems, *Chem. Phys. Lipids* 96 (1998) 141–157, [https://doi.org/10.1016/S0009-3084\(98\)00085-1](https://doi.org/10.1016/S0009-3084(98)00085-1).
- [40] B.M. Stott, M.P. Vu, C.O. McEmore, M.S. Lund, E. Gibbons, T.J. Bruseke, H.A. Wilson-Ashworth, J.D. Bell, Use of fluorescence to determine the effects of cholesterol on lipid behavior in sphingomyelin liposomes and erythrocyte membranes, *J. Lipid Res.* 49 (2008) 1202–1215, <https://doi.org/10.1194/jlr.M700479-JLR200>.
- [41] L. D'Auria, M. Fenaux, P. Aleksandrowicz, P. Van Der Smissen, C. Chantrian, C. Vermeylen, M. Vikkula, P.J. Courtroy, D. Tyteca, Micrometric segregation of fluorescent membrane lipids: relevance for endogenous lipids and biogenesis in erythrocytes, *J. Lipid Res.* 54 (2013) 1066–1076, <https://doi.org/10.1194/jlr.M034314>.
- [42] M. M. Gao, P.M. Lau, S.K. Kong, Mitochondrial toxin betulinic acid induces in vitro eryptosis in human red blood cells through membrane permeabilization, *Arch. Toxicol.* 88 (2014) 755–768, <https://doi.org/10.1007/s00204-013-1162-x>.
- [43] C. Leonard, L. Conrard, M. Guthmann, H. Pollet, M. Carquin, C. Vermeylen, P. Gailly, P. Van Der Smissen, M.P. Mingeot-Leclercq, D. Tyteca, Contributions of plasma membrane lipid domains to red blood cell (re) shaping, *Sci. Rep.* 7 (2017) art. 4264. doi:<https://doi.org/10.1038/s41598-017-04388-z>.
- [44] M. Carquin, L. Conrard, H. Pollet, P. Van Der Smissen, A. Cominelli, M. Veiga-da-Cunha, P.J. Courtroy, D. Tyteca, Cholesterol segregates into submicrometric domains at the living erythrocyte membrane: evidence and regulation, *Cell. Mol. Life Sci.* 72 (2015) 4633–4651, <https://doi.org/10.1007/s00018-015-1951-x>.
- [45] W. Rodgers, M. Glaser, Characterization of lipid domains in erythrocyte membranes, *Proc. Natl. Acad. Sci. U. S. A.* 88 (1991) 1364–1368, <https://doi.org/10.1073/pnas.88.4.1364>.
- [46] W. Rodgers, M. Glaser, Distributions of proteins and lipids in the erythrocyte membrane, *Biochemistry* 32 (1993) 12591–12598, <https://doi.org/10.1021/bi00210a007>.
- [47] A.C. Dumitru, M.A. Poncin, L. Conrard, Y.F. Dufrière, D. Tyteca, D. Alsteens, Nanoscale membrane architecture of healthy and pathological red blood cells, *Nanoscale Horiz.* 3 (2018) 293–304, <https://doi.org/10.1039/c7nh00187h>.
- [48] S.A. Sanchez, M.A. Triccerri, E. Gratton, Laurdan generalized polarization fluctuations measures membrane packing micro-heterogeneity in vivo, *Proc. Natl. Acad. Sci. U. S. A.* 109 (2012) 7314–7319, <https://doi.org/10.1073/pnas.1118288109>.
- [49] I. Mikhaylov, A. Samsonov, Lipid raft detecting in membranes of live erythrocytes, *Biochim. Biophys. Acta Biomembr.* 1808 (2011) 1930–1939, <https://doi.org/10.1016/j.bbame.2011.04.002>.
- [50] H. Ahyaouch, A.B. García-Arribas, J. Sot, E.J. González-Ramírez, J.V. Busto, B.G. Monasterio, N. Jiménez-Rojo, F.X. Contreras, A. Rendón-Ramírez, C. Martin, A. Alonso, F. Goñi, Pb (II) induces scramblase activation and ceramide-domain generation in red blood cells, *Sci. Rep.* 8 (2018) art. 7456. doi:<https://doi.org/10.1038/s41598-018-25905-8>.
- [51] I. Levental, M. Grzybek, K. Simons, Raft domains of variable properties and compositions in plasma membrane vesicles, *Proc. Natl. Acad. Sci. U. S. A.* 108 (2011) 11411–11416, <https://doi.org/10.1073/pnas.1105996108>.
- [52] G.W. Feigenson, Phase boundaries and biological membranes, *Annu. Rev. Biophys. Biomol. Struct.* 36 (2007) 63–77, <https://doi.org/10.1146/annurev.biophys.36.040306.132721>.
- [53] M. Seigneuret, P.F. Devaux, ATP-dependent asymmetric distribution of spin-labeled phospholipids in the erythrocyte membrane: relation to shape changes, *Proc. Natl. Acad. Sci. U. S. A.* 81 (1984) 3751–3755, <https://doi.org/10.1073/pnas.81.12.3751>.
- [54] J. Connor, C.C. Pak, A.J. Schroit, Exposure of phosphatidylserine in the outer leaflet of human red blood cells, *J. Biol. Chem.* 269 (1994) 2399–2404.
- [55] H.P. Duwe, E. Sackmann, Bending elasticity and thermal excitations of lipid bilayer vesicle: modulation by solutes, *Physica A* 163 (1990) 410–428, [https://doi.org/10.1016/0378-4371\(90\)90349-W](https://doi.org/10.1016/0378-4371(90)90349-W).
- [56] Y.-S. Ryu, D. Yoo, N.J. Wittenberg, J.-H. Suh, S.-W. Lee, Y. Sohn, S.-H. Oh, A.N. Parikh, S.-D. Lee, Continuity of monolayer-bilayer junctions for localization of lipid raft microdomains in model membranes, *Sci. Rep.* 6 (2016) 26823, <https://doi.org/10.1038/srep26823>.
- [57] N. Kučerka, M.-P. Nieh, J. Katsaras, Asymmetric distribution of cholesterol in unilamellar vesicles of monounsaturated phospholipids, *Langmuir* 25 (2009) 13522–13527, <https://doi.org/10.1021/la9020299>.
- [58] T. Baba, N. Terada, Y. Fujii, N. Ohno, S. Ohno, S.B. Sato, Ultrastructural study of echinocytes induced by poly(ethylene glycol)-cholesterol, *Histochem. Cell Biol.* 122 (2004) 587–592, <https://doi.org/10.1007/s00418-004-0723-8>.
- [59] B. Bicalho, J.L. Holovati, J.P. Packer, Phospholipidomics reveals differences in glycerophosphoserine profiles of hypothermally stored red blood cells and microvesicles, *Biochim. Biophys. Acta* 1828 (2013) 317–326, <https://doi.org/10.1016/j.bbame.2012.10.026>.
- [60] U. Salzer, R. Zhu, M. Luten, H. Isobe, V. Pastushenko, T. Perkmann, P. Hinterdorfer, G.J.C.G.M. Bosman, Vesicles generated during storage of red cells are rich in the lipid raft marker stomatin, *Transfusion* 48 (2008) 451–462, <https://doi.org/10.1111/j.1537-2995.2007.01549.x>.
- [61] B. Chailley, F. Giraud, M. Claret, Alterations in human erythrocyte shape and the state of spectrin and phospholipid phosphorylation induced by cholesterol depletion, *Biochim. Biophys. Acta* 643 (1981) 636–641, [https://doi.org/10.1016/0005-2736\(81\)90359-X](https://doi.org/10.1016/0005-2736(81)90359-X).
- [62] K. Motoyama, H. Toyodome, R. Onodera, T. Irie, F. Hirayama, K. Uekama, H. Arima, Involvement of lipid rafts of rabbit red blood cells in morphological changes induced by methylated  $\beta$ -cyclodextrins, *Biol. Pharm. Bull.* 32 (2009) 700–705, <https://doi.org/10.1248/bpb.32.700>.
- [63] R. van Zwieten, A.E. Bochem, P.M. Hilarius, R. van Bruggen, F. Bergkamp, G.K. Hovingh, A.J. Verhoeven, The cholesterol content of the erythrocyte membrane is an important determinant of phosphatidylserine exposure, *Biochim. Biophys. Acta* 1821 (2012) 1493–1500, <https://doi.org/10.1016/j.bbailip.2012.08.008>.
- [64] R. Lipowsky, D. Dimova, Domains in membranes and vesicles, *J. Phys. Condens. Matter* 15 (2003) S31–S45, <https://doi.org/10.1088/0953-8984/15/1/304>.
- [65] V.A.J. Frolow, Y.A. Chizmadzhev, F.S. Cohen, J. Zimmerberg, "Entropic traps" in the kinetics of phase separation in multicomponent membranes stabilize nanodomains, *Biophys. J.* 91 (2006) 189–205, <https://doi.org/10.1529/biophysj.105.068502>.
- [66] T. Baumgart, S. Das, W.W. Webb, J.T. Jenkins, Membrane elasticity in giant vesicles with fluid phase coexistence, *Biophys. J.* 89 (2005) 1067–1080, <https://doi.org/10.1529/biophysj.104.049692>.
- [67] S. Semrau, Idema, T., Holtzer, L., Schmidt, T., C. Storm, Accurate determination of elastic parameters for multicomponent membranes, *Phys. Rev. Lett.* 11 (2008) art. 088101. doi:<https://doi.org/10.1103/PhysRevLett.100.088101>.
- [68] A.R. Honerkamp-Smith, M.D. P. Cicuta, S.L. Collins, M. den Nijs Veatch, M. Schick, S.L. Keller, Line tension, correlation lengths, and critical exponents in lipid

- membrane near critical points, *Biophys. J.* 95 (2008) 236–246, <https://doi.org/10.1529/biophysj.107.128421>.
- [69] R.E. Waugh, Elastic energy of curvature-driven bump formation on red blood cell membrane, *Biophys. J.* 70 (1996) 1027–1035, [https://doi.org/10.1016/S0006-3495\(96\)79648-0](https://doi.org/10.1016/S0006-3495(96)79648-0).
- [70] R.E. Waugh, R.G. Bauserman, Physical measurements of bilayer-skeletal separation forces, *Ann. Biomed. Eng.* 23 (1995) 308–321, <https://doi.org/10.1007/BF02584431>.
- [71] Y. Park, C.A. Best, K. Badizadegan, R.R. Dasari, M.S. Feld, T. Kuriabova, M.L. Henle, A.J. Levine, G. Popescu, Measurement of red blood cell mechanics during morphological changes, *Proc. Natl. Acad. Sci. U. S. A.* 107 (2010) 6731–6736, <https://doi.org/10.1073/pnas.0909533107>.
- [72] M. Göllner, A.C. Toma, N. Strelnikova, S. Deshpande, T. Pfohl, A self-filling microfluidic device for noninvasive time-resolved single red blood cell experiments, *Biomicrofluidics* 10 (2016) art. 054121. doi:<https://doi.org/10.1063/1.4966212>.
- [73] E.A. Evans, Bending elastic modulus of red blood cell membrane derived from buckling instability in micropipet aspiration assays, *Biophys. J.* 43 (1983) 27–30, [https://doi.org/10.1016/S0006-3495\(83\)84319-7](https://doi.org/10.1016/S0006-3495(83)84319-7).
- [74] J. Evans, W. Gratzner, N. Mohandas, K. Parker, J. Sleep, Fluctuation of the red blood cell membrane: relation to mechanical properties and lack of ATP dependence, *Biophys. J.* 94 (2008) 4134–4144, <https://doi.org/10.1529/biophysj.107.117952>.
- [75] J.K. Khodadad, R.S. Weinstein, The band 3-rich membrane of llama erythrocytes: studies on cell shape and the organization of membrane proteins, *J. Membrane Biol.* 72 (1983) 161–171, <https://doi.org/10.1007/BF01870583>.
- [76] J.E. Ferrell, K.-J. Lee, W.H. Huestis, Membrane bilayer balance and erythrocyte shape: a quantitative assessment, *Biochemistry* 24 (1985) 2849–2857, <https://doi.org/10.1021/bi00333a006>.
- [77] N. Mohandas, E. Evans, Mechanical properties of the red cell membrane in relation to molecular structure and genetic defects, *Annu. Rev. Biophys. Biomol. Struct.* 23 (1994) 787–818, <https://doi.org/10.1146/annurev.bb.23.060194.004035>.
- [78] M. Deserno, Fluid lipid membranes: from differential geometry to curvature stress, *Chem. Phys. Lipids* 185 (2015) 11–45, <https://doi.org/10.1016/j.chemphyslip.2014.05.001>.
- [79] W. Wang, L. Yang, H.W. Huang, Evidence of cholesterol accumulated in high curvature regions: implication to the curvature elastic energy for lipid mixtures, *Biophys. J.* 92 (2007) 2819–2830, <https://doi.org/10.1529/biophysj.106.097923>.

## Repository KITopen

Dies ist ein Postprint/begutachtetes Manuskript.

Empfohlene Zitierung:

Melzak, K. A.; Moreno-Flores, S.; Bieback, K.

[Spicule movement on RBCs during echinocyte formation and possible segregation in the RBC membrane](#)

2020. Biochimica et biophysica acta / Biomembranes, 1862

[doi: 10.554/IR/1000120975](#)

Zitierung der Originalveröffentlichung:

Melzak, K. A.; Moreno-Flores, S.; Bieback, K.

[Spicule movement on RBCs during echinocyte formation and possible segregation in the RBC membrane](#)

2020. Biochimica et biophysica acta / Biomembranes, 1862 (10), Article No. 183338.

[doi:10.1016/j.bbamem.2020.183338](#)